



HAL
open science

High mobility InGaAs/InAlAs pseudomorphic heterostructures on InP(001)

X. Wallart, B. Pinsard, F. Mollot

► **To cite this version:**

X. Wallart, B. Pinsard, F. Mollot. High mobility InGaAs/InAlAs pseudomorphic heterostructures on InP(001). Journal of Applied Physics, 2005, 97, pp.053706-1-6. hal-00125384

HAL Id: hal-00125384

<https://hal.science/hal-00125384>

Submitted on 25 May 2022

HAL is a multi-disciplinary open access archive for the deposit and dissemination of scientific research documents, whether they are published or not. The documents may come from teaching and research institutions in France or abroad, or from public or private research centers.

L'archive ouverte pluridisciplinaire **HAL**, est destinée au dépôt et à la diffusion de documents scientifiques de niveau recherche, publiés ou non, émanant des établissements d'enseignement et de recherche français ou étrangers, des laboratoires publics ou privés.

High-mobility InGaAs / InAlAs pseudomorphic heterostructures on InP (001)

Cite as: J. Appl. Phys. **97**, 053706 (2005); <https://doi.org/10.1063/1.1858871>

Submitted: 22 September 2004 • Accepted: 17 December 2004 • Published Online: 15 February 2005

X. Wallart, B. Pinsard and F. Mollot



View Online



Export Citation

ARTICLES YOU MAY BE INTERESTED IN

[Band parameters for III-V compound semiconductors and their alloys](#)

Journal of Applied Physics **89**, 5815 (2001); <https://doi.org/10.1063/1.1368156>

[Review Article: Molecular beam epitaxy of lattice-matched InAlAs and InGaAs layers on InP \(111\)A, \(111\)B, and \(110\)](#)

Journal of Vacuum Science & Technology B **35**, 010801 (2017); <https://doi.org/10.1116/1.4972049>

[The growth of high mobility InGaAs and InAlAs layers by molecular beam epitaxy](#)

Journal of Vacuum Science & Technology B: Microelectronics Processing and Phenomena **4**, 536 (1986); <https://doi.org/10.1116/1.583421>

Lock-in Amplifiers
up to 600 MHz



Zurich
Instruments



High-mobility InGaAs/InAlAs pseudomorphic heterostructures on InP (001)

X. Wallart,^{a)} B. Pinsard, and F. Mollot

Institut d'Electronique, de Microelectronique et de Nanotechnologie, Unité Mixte de Recherche (UMR) 8520 Centre National de la Recherche Scientifique (CNRS), Avenue Poincaré, 59652 Villeneuve d'Ascq Cedex, France

(Received 22 September 2004; accepted 17 December 2004; published online 15 February 2005)

In this work, we study the growth of strained $\text{In}_x\text{Ga}_{1-x}\text{As}$ alloys on InP by gas source molecular-beam epitaxy in the 350–500 °C range. At low temperatures, we show that the As-rich (2×3) surface reconstruction promotes three-dimensional growth mode whereas the less As-rich (2×4) and cation-rich ones allow keeping two-dimensional growth. For heterostructures with a lattice-matched InAlAs barrier and a strained $\text{In}_{0.75}\text{Ga}_{0.25}\text{As}$ channel, grown at 500 °C, the electron mobility rises to 16 000 and 139 000 $\text{cm}^2/\text{V s}$ at 300 and 77 K, respectively, for a 140-Å-thick channel layer and a 400-Å-thick spacer layer. Both values are among the best ones ever reported for an InGaAs/InAlAs heterostructure. © 2005 American Institute of Physics. [DOI: 10.1063/1.1858871]

I. INTRODUCTION

High-speed microelectronics such as high electron mobility transistors (HEMTs) or ballistic devices require low electron mass/high-mobility active layers. Among III-V semiconductors, high In content (x_{In}) $\text{In}_x\text{Ga}_{1-x}\text{As}$ alloys have long been recognized as materials of interest.^{1,2} This implies either the pseudomorphic growth on InP substrates or the metamorphic one on GaAs or InP substrates. We focus here on the first approach. Previous work in this field studied the detailed mechanisms of the pseudomorphic growth or reported transport results on specific heterostructures. As regards the strained growth, the two strain relaxation mechanisms have been identified with their corresponding critical thickness. Under As-stabilized conditions and for a growth temperature around 500 °C, plastic relaxation occurs via dislocation nucleation for x_{In} below 0.75–0.8. On the contrary, elastic relaxation characterized by a two-dimensional (2D) to a three-dimensional (3D) growth mode transition is detected for x_{In} above 0.8.^{3–8} The effects of growth kinetics were also evidenced. A reduction of the growth temperature allows an increase of the critical thickness for a given x_{In} while a change in surface reconstruction can induce a change in the relaxation mechanism.⁹ From these previous studies, there is a general agreement to consider that the highest x_{In} which allows the growth of a good quality pseudomorphic channel, typically 10–15 nm thick, lies around 0.75. This is confirmed by the electron mobility results obtained for x_{In} around 0.75.^{10–14} For InAlAs/ $\text{In}_x\text{Ga}_{1-x}\text{As}$ heterostructures, Tacano and co-workers^{10,11} have reported electron mobility values of 16 000, 112 000, and 160 000 $\text{cm}^2/\text{V s}$ at 300, 77, and 10 K, respectively, for $x_{\text{In}}=0.8$. For a slightly lower x_{In} of 0.75, Drouot *et al.*¹² got 12 000, 110 000, and 170 000 $\text{cm}^2/\text{V s}$ at 300, 77, and 4 K, respectively. The 300 K electron mobility obtained by Nakayama and Miyamoto¹³ reached 18 500 $\text{cm}^2/\text{V s}$ using a composite channel made of a 13-nm-thick lattice-matched InGaAs layer

below a 7-nm-thick InAs one, although this latter thickness is around twice the critical one for the growth of InAs on InP. Unfortunately, the authors did not report any low-temperature mobility value. Finally, Ramvall *et al.*¹⁴ measured a low-temperature mobility value at 170 000 and 520 000 $\text{cm}^2/\text{V s}$ at 77 K and 300 mK, respectively, for $x_{\text{In}}=0.75$. In this case, the barrier material is no longer the lattice-matched InAlAs alloy but InP.

In this context, the first goal of this work is to determine to what extent a decrease of the surface kinetics via a lowering of the growth temperature can allow to further increase x_{In} while avoiding strain relaxation of the active layer. Previous attempts have been restricted to growth temperatures around 450 °C; we want to go further. The second objective of this work is to study the effect of the structure parameters such as the channel and the spacer thicknesses and the 2D electron gas concentration on the transport properties, especially the electron mobility.

II. EXPERIMENT

Epitaxial layers are grown by gas source molecular-beam epitaxy (GSMBE) using cracked AsH_3 in a Riber MBE 32 system. Growth rates in the 0.5–1 monolayer (ML)s range and layer composition are determined by reflection high-energy electron diffraction (RHEED) intensity oscillations. Strained InGaAs layers are grown on a 300-nm-thick lattice-matched InAlAs buffer on InP grown at 510 °C under As-rich conditions (2×1 reconstruction). The substrate temperature is then lowered down to the desired growth temperature of the InGaAs layer under an As flux. The onset of 3D growth or surface roughening is detected by recording the intensity of a 3D diffraction spot. After growth, the samples are characterized “*ex situ*” by Hall-effect measurements at 300 and 77 K, atomic force microscopy (AFM), and photoluminescence (PL).

^{a)}Electronic mail: xavier.wallart@iemn.univ-lille.fr

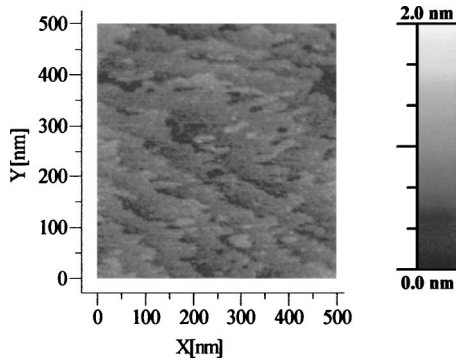


FIG. 1. AFM image of the 3000-Å-thick InAlAs buffer layer.

III. RESULTS AND DISCUSSION

We first discuss RHEED and AFM observations during the growth of a strained InGaAs layer at various temperatures before considering the Hall-effect measurements on heterostructures.

A. RHEED and AFM observations

We investigate an x_{In} range between 0.8 and 0.9 and mainly focus on the effect of the lowering of the growth temperature, here chosen between 350 and 450 °C. These temperatures are lower than the usual one of 500 °C in order to kinetically prevent the film relaxation as far as possible. Indeed, previous works^{3,9} have clearly established that around 500 °C, the critical thickness for x_{In} above 0.8 is significantly less than 100–150 Å which is the typical thickness of the active layer of a heterostructure. However, since the strained InGaAs layers are grown on a lattice-matched InAlAs buffer, it is worth looking first at the buffer surface morphology. Figure 1 shows an AFM image of a 3000-Å-thick InAlAs buffer. The surface is very flat and atomic steps are clearly resolved, separated by 500–1000-Å wide terraces. We conclude that this is a good starting surface for the growth of the strained layers and that the relaxation processes further observed are uniquely related to strain in the InGaAs layers.

In a first set of experiments, we choose a 1 SCCM (denotes cubic centimeter per minute at STP) AsH₃ flow rate at 350 and 400 °C and a 1.5 SCCM one at 450 °C. In our experimental conditions, 0.6 SCCM corresponds approximately to a 1 monolayer/s As impinging flux on the surface. The corresponding RHEED pattern exhibits either a 2×3 reconstruction at 350 °C or a 2×4 one at 400 and 450 °C at the beginning of the growth of the InGaAs strained layer. Then this pattern progressively weakens and the 3D spot intensity presents either a sharp increase, corresponding to the 2D to 3D growth mode transition, or a slow increase, corresponding to the surface roughening, the 2D growth being preserved. We then define two types of thickness: h_{3D} in the former case and h_r in the latter one. H_{3D} is related to the usual critical thickness for the onset of elastic relaxation. Gendry *et al.*³ have observed surface roughening before plastic relaxation that they have detected by RHEED streak spacing variations. More, they have shown that surface steps promote dislocation nucleation and reduce the critical

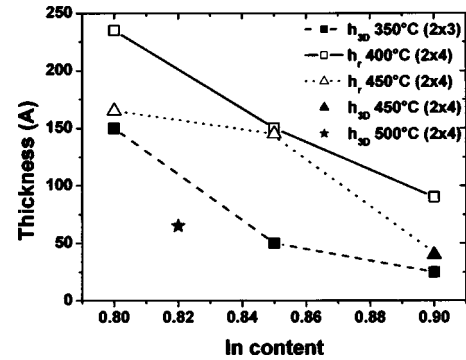


FIG. 2. Critical thickness for the onset of 3D growth mode (h_{3D}) or surface roughening (h_r) vs the In content of the strained InGaAs layer at different growth temperatures and for two surface reconstructions. The h_{3D} value at 500 °C, taken from Ref. 9, is added for comparison.

thickness.⁵ It suggests that surface roughening favors dislocation nucleation at surface defects. In the same way, Peiro *et al.*⁸ have noted a surface rippling with ripples along the [1–10] direction preceding plastic strain accommodation along the [1–10] one. Hence surface roughening could be considered as a precursor state and h_r as a lower limit for plastic relaxation. Figure 2 summarizes our results together with the value for h_{3D} at 500 °C and $x_{\text{In}}=0.82$ obtained by Gendry *et al.*^{3,9} for comparison. We note that at 350 °C, the onset of 3D growth is always detected whereas at 400 °C, the growth keeps its 2D character. At 450 °C, 3D growth is only observed for the highest In content.

AFM observations for thickness ranging from 200 to 500 Å confirm these RHEED findings, as illustrated in Fig. 3. At 350 °C, the formation of dots on the surface is clearly visible [Fig. 3(a)] whereas at 400 °C, the cross-hatched surface morphology, characteristic of plastic relaxation, is observed [Fig. 3(b)] At 450 °C, the AFM images stress the transition in the relaxation mode deduced from the RHEED patterns. Indeed, for $x_{\text{In}}=0.8$, the surface morphology is still 2D [Fig. 3(c)] whereas for $x_{\text{In}}=0.9$, 3D growth occurs [Fig. 3(d)].

A striking point in Fig. 2 is that the h_{3D} thickness at 350 °C is lower than the h_r one at 400 °C, which is not expected from the reduction of surface kinetics induced by a growth temperature lowering. However, at 350 °C, the surface reconstruction is different from that at 400 °C and this could be the reason for this behavior. We then perform a complementary set of experiments at 350 °C for $x_{\text{In}}=0.85$ with decreased AsH₃ flow rates in order to tune the surface reconstruction. We start with the above As-rich (2×3) one, go then to the less As rich (2×4), and end finally with the cation rich (4×2). For the two latter reconstructions, the 2D-3D transition is no longer detected in contrast to the 2×3 case. These results (Table I and Fig. 4) evidence the role of the surface reconstruction on the strain relaxation mechanism. Clearly, an As-rich reconstruction favors the onset of 3D growth even at 350 °C which is a low growth temperature. On the contrary, in less As-rich conditions, 2D growth mode is preserved and the critical thickness before the onset of surface roughening is delayed. This is related to the surface energy which is lower for an As-rich surface than for a cation-rich one. Hence, on As-rich surfaces, strain relaxation

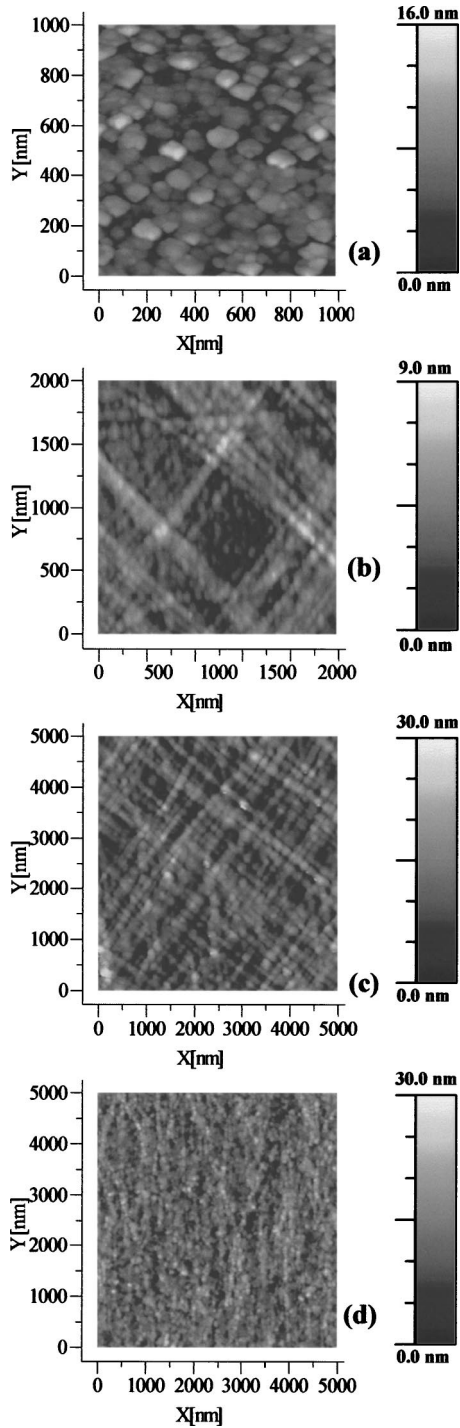


FIG. 3. AFM images of strained $\text{In}_x\text{Ga}_{1-x}\text{As}$ layers with $x_{\text{In}}=0.8$ grown at 350 °C (a), 400 °C (b), and 450 °C (c) and $x_{\text{In}}=0.9$ at 450 °C (d). The film thickness is 260 Å (a), 370 Å (b), 500 Å (c), and 200 Å (d).

via 3D growth mode transition is favored since the energy needed to create the related specific surface is low. This behavior has already been observed by Gendry *et al.*⁹ during the growth of $\text{In}_{0.82}\text{Ga}_{0.18}\text{As}$ at 525 °C on InP.

When used as an active layer of a heterostructure, the strained InGaAs channel thickness should be in the 100–150-Å range, i.e., the associated critical thickness should be higher than 150 Å. In light of the above results, it turns out that the In content must be limited below 0.85. As regards the substrate temperature, at 350 °C, the 2×3 recon-

TABLE I. Variations of $h_{3\text{D}}$ and h_r versus growth conditions at $T_g = 350$ °C (0.6 SCCM AsH_3 corresponds approximately to an As flux of 1 ML/s).

AsH_3 (SCCM)	Surface reconstruction	$h_{3\text{D}}$ (Å)	h_r (Å)
1	2×3	50	...
0.6	2×4	...	90
0.4	4×2	...	135

struction favors 3D growth and hence the 2×4 one must be preferred. However, even in this case, h_r is not larger at 350 °C than at 400 °C although the surface kinetics is reduced. We attribute this to short-range roughening associated with insufficient surface diffusion of impinging atoms at 350 °C. In other words, the growth temperature lowering which is expected to delay strain relaxation reaches the limit for which it impedes surface diffusion and hence induces surface roughening. Then, depending on the surface reconstruction, this surface roughening is a precursor state either

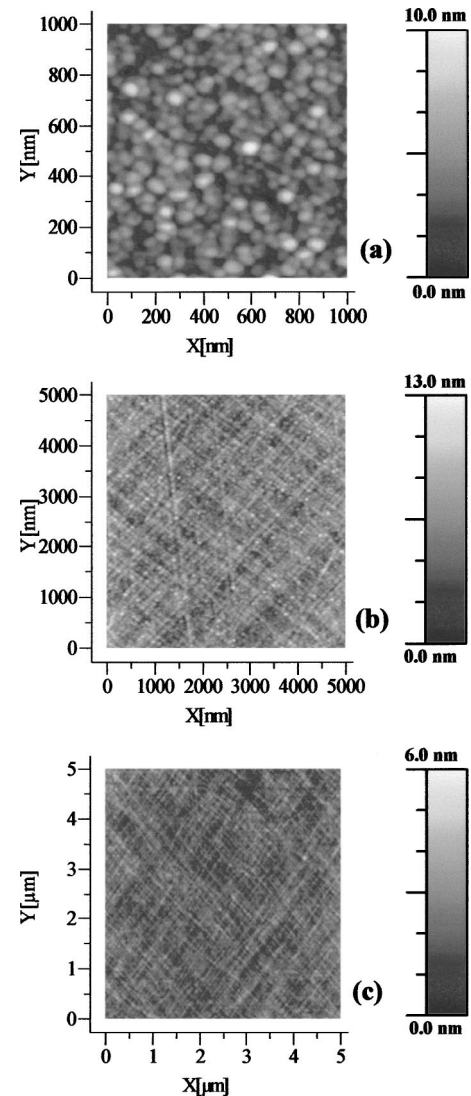


FIG. 4. AFM images of strained $\text{In}_x\text{Ga}_{1-x}\text{As}$ layers with $x_{\text{In}}=0.85$ at 350 °C exhibiting a 2×3 reconstruction (a), a 2×4 one (b), and a 4×2 one (c). The film thickness is 120 Å (a), 340 Å (b), and 440 Å (c).

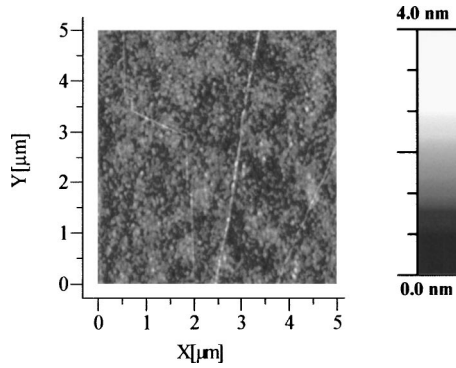


FIG. 5. AFM image of a 120-Å-thick $\text{In}_{0.82}\text{Ga}_{0.18}\text{As}$ layer grown at 450 °C.

for 3D growth (2×3 case) or dislocation nucleation and plastic relaxation (2×4 and 4×2 cases). Hence in the following, we do not consider anymore the 350 °C growth but focus only on the 400 and 450 °C growth temperatures.

For $T_g=400$ and 450 °C and x_{In} around 0.85, RHEED observations only provide the thickness for surface roughening. As discussed above, this is not directly a measurement of the onset of plastic relaxation. Then, considering that we are interested in 100–150-Å-thick active layers, we perform complementary AFM measurements on four strained layers, 120 Å thick. Two of them are grown at 400 °C, with $x_{\text{In}}=0.88$ and 0.85, the two others are grown at 450 °C with $x_{\text{In}}=0.85$ and 0.82. For these four samples, the AFM images are quite similar and look like that in Fig. 5. The surface morphology is rather flat but characterized by the appearance of line defects, not observed on the buffer layer surface (see Fig. 1), related to the beginning of strain relaxation. Hence the onset of plastic relaxation appears below 120 Å in these cases. This in turn implies that the critical thickness for plastic relaxation has been overestimated by the above h_r determination. Nevertheless, it does not imply that plastic relaxation occurs before surface roughening but that this latter begins for thickness below those we have detected in Fig. 2. This is probably due to the experimental uncertainty in the determination of h_r since as previously mentioned, the 3D spot intensity increase in this case is smooth. Anyway, this

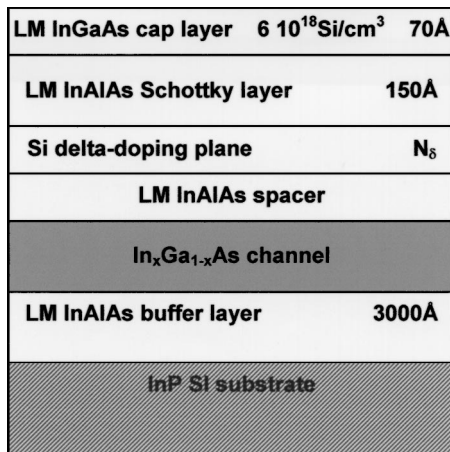


FIG. 6. Typical vertical structure used for Hall-effect measurements (LM indicates that the corresponding layer is lattice matched to InP). N_δ has been varied from 6×10^{11} to $4.5 \times 10^{12} \text{ cm}^{-2}$.

TABLE II. Electron mobility results for structures grown at T_g ranging from 400 to 500 °C with $0.8 < x_{\text{In}} < 0.85$.

Sample	Channel thickness (Å)	μ ($\text{cm}^2/\text{V s}$) at 300 K	μ ($\text{cm}^2/\text{V s}$) at 77 K
$T_g=400$ °C/ $x_{\text{In}}=0.85$	100	10 700	27 900
$T_g=450$ °C/ $x_{\text{In}}=0.82$	100	10 700	32 700
$T_g=450$ °C/ $x_{\text{In}}=0.80$	120	13 900	59 900
$T_g=500$ °C/ $x_{\text{In}}=0.80$	120	15 000	81 900

suggests that plastic relaxation starts quite rapidly after surface roughening which agrees well with the results of Peiro *et al.*⁸

B. Heterostructures: Material parameters

We then complete the above analysis with Hall-effect measurements on heterostructures. Figure 6 shows the typical layer sequence. In the first set, we grow 100-Å-thick channel heterostructures with $x_{\text{In}}=0.85$ at 400 °C and $x_{\text{In}}=0.82$ at 450 °C. According to the above results, 120-Å-thick strained layers have begun to relax. It is then interesting to know how this early stage of relaxation affects the electron mobility. In both cases, the spacer thickness is 400 Å and the delta-doping plane value is $2 \times 10^{12} \text{ cm}^{-2}$. The Hall mobility results are displayed in Table II (first two lines). The electron mobility is lower than expected in both cases. In the second set, we then reduce the In content to 0.8 and perform the channel growth at 450 and 500 °C which is the usual growth temperature for such structures. The results are displayed in Table II (lines 3 and 4) and show that the 500 °C growth temperature is the best one. The measured mobility value for $x_{\text{In}}=0.8$ and $T_g=500$ °C is the best of Table II although decreasing x_{In} is expected to induce a mobility decrease, which is not the case here. This confirms that the relaxation observed for layers with $x_{\text{In}}=0.82$ and 0.85 (Fig. 5) is sufficient to affect significantly the electron mobility. As regards the growth temperature, the unavoidable growth interruption needed to lower the channel growth temperature seems to be detrimental for the transport properties.

We then concentrate on heterostructures grown at 500 °C with two more samples with $x_{\text{In}}=0.75$ and 0.77. The results are displayed in Fig. 7. The $x_{\text{In}}=0.8$ sample is clearly worse than the two others both at 77 and 300 K. Together with the 10-K PL measurements in Fig. 8, this shows that the

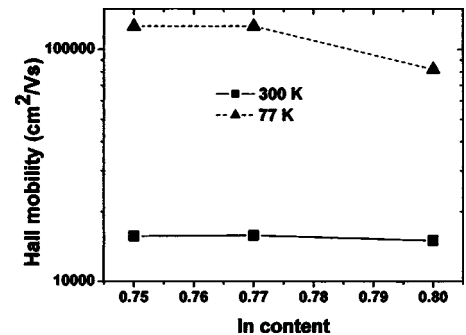


FIG. 7. Electron mobility for 120-Å-thick channel heterostructures grown at 500 °C for various In content at 300 and 77 K.

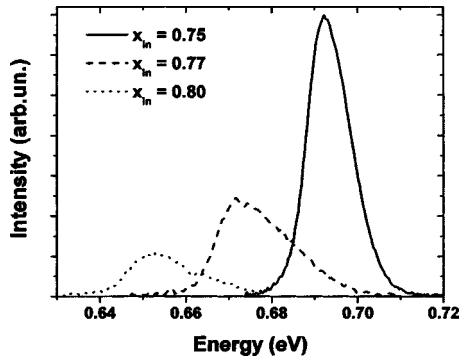


FIG. 8. 10-K photoluminescence spectra recorded on 120-Å-thick channel heterostructures grown at 500 °C.

channel layer plastic relaxation has already occurred. Indeed, the PL intensity of the $x_{\text{In}}=0.80$ sample is lower than that in the two other ones, demonstrating a high dislocation density in the channel. On the contrary, the total integrated intensity is quite similar for $x_{\text{In}}=0.75$ and 0.77 although the PL peak is broader in the latter case. This broadening could be related to the surface roughening occurring for $x_{\text{In}}=0.77$. This only slightly degrades the electron mobility. The effective mass decrease when going from $x_{\text{In}}=0.75$ to $x_{\text{In}}=0.77$ compensates this effect in such a way that the electron mobility is similar in both cases. This picture at a fixed thickness for increasing In content is complementary to that obtained at a fixed In content and increasing thickness. In both cases, starting with almost ideal pseudomorphic growth, when increasing either the In content or the thickness, the sample surface first roughens before dislocations nucleate and plastic relaxation takes place.

C. Heterostructures: Effect of structure parameters

The above results on heterostructures indicate that the best electron mobility is achieved for $x_{\text{In}}=0.75$ and a growth temperature of 500 °C. Within these growth conditions, we have then tested the effect of three structure parameters, i.e., the 2D electron gas density (N_s), the spacer, and the channel thickness, on the electron mobility.

The variations of the electron mobility with the sheet carrier density (N_s) are reported in Fig. 9(a). We use structures with a 120-Å-thick channel and a variable Si delta-doping plane from 6×10^{11} to 4.5×10^{12} cm $^{-2}$. For the three lowest N_s values, we use a 400-Å-thick spacer layer whereas for the highest value, the spacer is 200 Å thick. We observe an increase of the electron mobility towards a sheet carrier density of 8×10^{11} cm $^{-2}$ although the interaction between ionized impurities and the electron gas increases with larger delta-doping planes. This is attributed to many-body effects in the 2D electron gas which result in a screening of the various scattering mechanisms. This screening is more efficient at relatively large densities. Above 8×10^{11} cm $^{-2}$, the observed saturation can be due to alloy scattering which tends to be the dominant limiting factor of the mobility¹⁴ and/or to the reduced spacer thickness used for the highest N_s value. Nevertheless, with $N_s=1.65 \times 10^{12}$ cm $^{-2}$, we get an electron mobility of 15 700 and 129 000 cm 2 /V s at 300 and

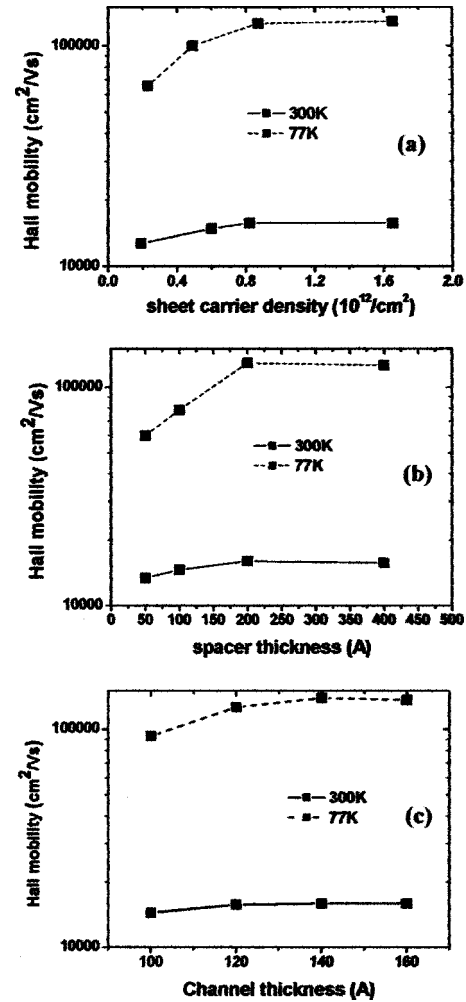


FIG. 9. Electron mobility at 300 and 77 K vs sheet carrier density (a), spacer thickness (b), and channel thickness (c), for heterostructures with 75% In content channel.

77 K, respectively. These values lead to a very interesting $N_s x \mu$ product which is the relevant quantity for most device applications.

Figure 9(b) show the increase of the mobility with the spacer thickness. These results are measured on structures with 120-Å-thick channel layer for which the sheet carrier density is above 8×10^{11} cm $^{-2}$. The observed evolution is expected since the interaction of the 2D gas electrons with the remote ionized impurities decreases with the spacer thickness. However, above 200 Å, the mobility saturates, indicating that scattering by the ionized donor is not the limiting factor anymore. Indeed, at 77 K, once again, alloy scattering has to be considered as the preponderant limiting factor for the mobility.

The variations of the mobility with the channel thickness are depicted in Fig. 9(c) for heterostructures with a 400-Å-thick spacer layer and a 2×10^{12} cm $^{-2}$ Si delta-doping plane. The mobility improvement observed towards 140 Å is due to a reduction of interface scattering with increasing thickness. Above 140 Å, the mobility does not increase anymore: this can be attributed to saturation of the previous mechanism as well as to surface roughening and/or the very beginning of plastic relaxation. Under these conditions, the

best mobility values we get are 16 000 and 139 000 $\text{cm}^2/\text{V s}$ at 300 and 77 K with a corresponding N_s value of $8.5 \times 10^{11} \text{ cm}^{-2}$. To our knowledge, these values are among the best ones ever reported for AlInAs/GaInAs heterostructures grown by MBE. Nakayama and Miyamoto¹³ have reported a higher room-temperature mobility of 18 500 $\text{cm}^2/\text{V s}$ with a rather high N_s of $3.1 \times 10^{12} \text{ cm}^{-2}$ but no 77 K results. Ramvall *et al.*¹⁴ got 16 000 and 170 000 $\text{cm}^2/\text{V s}$ at 300 and 77 K, respectively, with N_s around $6.5 \times 10^{11} \text{ cm}^{-2}$ on metal-organic chemical-vapor deposition (MOCVD)-grown heterostructures using a 90-Å channel layer and InP as spacer and barrier material. Since the conduction-band offset at the InP/InGaAs heterojunction is lower than that at the InAlAs/InGaAs one, interface roughness, even if similar in both cases, will induce lower electron-scattering effects in the InP/InGaAs case. More, the part of the electronic transport occurring in the barrier (due to the unavoidable electron wave-function penetration in the barrier) takes advantage of the higher electron mobility of InP with respect to InAlAs, especially at 77 K since InP is a binary compound. We think that both effects can account for the higher value reported by Ramvall *et al.*

IV. CONCLUSION

This study shows that the reduction of surface kinetics via growth temperature lowering does not allow increasing significantly the In content of the active layer of devices. More, it evidences the role of surface reconstruction on the strain relief mechanism for a growth temperature of 350 °C. Using the best growth temperature (500 °C) and the highest possible In content (0.75), we study the influence of the structure design on the electron mobility which reaches 16 000 and 139 000 $\text{cm}^2/\text{V s}$ at 300 and 77 K, respectively, with a corresponding N_s of $8.5 \times 10^{11} \text{ cm}^{-2}$ for an optimized

structure. These values are among the best reported for the InGaAs/InAlAs system. If the $N_s x \mu$ product is the most relevant quantity, we show that a 200-Å-thick spacer layer together with a $4.5 \times 10^{12} \text{ cm}^{-2}$ Si delta-doping plane allow to significantly increase N_s ($1.65 \times 10^{12} \text{ cm}^{-2}$) while keeping a high electron mobility.

ACKNOWLEDGMENTS

The authors are grateful to C. Coinon for his help in the sample MBE growth, to J. L. Codron for the Hall-effect measurements, and to Dr. D. Vignaud for the photoluminescence experiments.

- ¹J. Massies, J. Rochette, P. Delescluse, P. Etienne, J. Chevrier, and N. T. Linh, *Electron. Lett.* **18**, 758 (1982).
- ²J. Massies and M. Sauvage-Simkin, *Appl. Phys. A: Solids Surf.* **32**, 27 (1983).
- ³M. Gendry, V. Drouot, C. Santinelli, G. Hollinger, C. Miozzi, and M. Pitaval, *J. Vac. Sci. Technol. B* **10**, 1829 (1992).
- ⁴S. Z. Chang, S. C. Lee, C. R. Chen, and L. J. Chen, *J. Appl. Phys.* **75**, 1511 (1994).
- ⁵S. Jourba, M. Gendry, P. Regreny, and G. Hollinger, *J. Cryst. Growth* **201/202**, 1101 (1999).
- ⁶D. Lacombe, A. Ponchet, S. Fréchengues, V. Drouot, N. Bertru, B. Lambert, and A. Le Corre, *J. Cryst. Growth* **201/202**, 252 (1999).
- ⁷M. Gendry, V. Drouot, G. Hollinger, and S. Mahajan, *Appl. Phys. Lett.* **66**, 40 (1995).
- ⁸F. Peiro, A. Cornet, M. Beck, and M. A. Py, *Appl. Phys. Lett.* **74**, 3818 (1999).
- ⁹M. Gendry, G. Grenet, Y. Robach, P. Krapf, L. Porte, and G. Hollinger, *Phys. Rev. B* **56**, 9271 (1997).
- ¹⁰M. Tacano, Y. Sugiyama, Y. Takeuchi, and Y. Ueno, *J. Electron. Mater.* **20**, 1081 (1991).
- ¹¹Y. Sugiyama, Y. Takeuchi, and M. Tacano, *J. Cryst. Growth* **115**, 509 (1991).
- ¹²V. Drouot, M. Gendry, C. Santinelli, P. Viktorovitch, and G. Hollinger, *J. Appl. Phys.* **77**, 1810 (1995).
- ¹³T. Nakayama and H. Miyamoto, *J. Cryst. Growth* **201/202**, 782 (1999).
- ¹⁴P. Ramvall, N. Carlsson, P. Omling, L. Samuelson, W. Seifert, M. Stolze, and Q. Wang, *Appl. Phys. Lett.* **68**, 1111 (1996).